Dynamics of D_3^+ slow dissociation induced by intense ultrashort laser pulses

B. Gaire, J. McKenna, M. Zohrabi, K. D. Carnes, B. D. Esry, and I. Ben-Itzhak
J.R. Macdonald Laboratory, Physics Department, Kansas State University, Manhattan, Kansas 66506, USA
(Received 12 December 2011; published 21 February 2012)

The dissociation of D_3^+ in intense ultrashort laser pulses is investigated using an improved coincidence three-dimensional momentum imaging method that allows clear separation of all fragmentation channels and the determination of the kinetic energy release down to zero. Our results, using 10-fs, 790-nm pulses, suggest that a large peak at low kinetic energy release is associated with the $D^+ + D_2$ dissociation channel of D_3^+. The most likely dissociation pathways leading to two-body breakup of D_3^+ are identified with additional measurements using 25-fs, 790-nm and 40-fs, 395-nm pulses. We also show that the slow $D^+ + D_2$ dissociation dynamics can be manipulated by the pulse duration.

DOI: 10.1103/PhysRevA.85.023419 PACS number(s): 33.80.Rv, 42.50.Hz

I. INTRODUCTION

The triatomic hydrogen molecular ion H_3^+ is one of the major constituents of the universe and is important on a fundamental level. This fact has motivated a multitude of laboratory studies on this species, such as studies of dissociative recombination of H_3^+ conducted in storage rings (e.g., [1–5]), dissociative collisions (e.g., [6–8]), and weak-field laser spectroscopy [9,10]. For similar reasons, exploring the nonlinear behavior of H_3^+ (or D_3^+) in ultrashort intense laser fields is desirable as it can lead to a better understanding of the laser-driven dynamics of polyatomic molecules—in a similar way that H_2^+ has been a benchmark system for studies of diatomic molecules [11,12].

Until recently there were no published experimental studies on H_3^+ and its isotopologues in intense ultrashort laser fields. A couple of years ago, we reported measurements of D_3^+ dynamics measured by coincidence three-dimensional momentum imaging [13]. The focus of that work was on the ionization channels, namely the fragmentation of the transient D_3^{2+} and D_3^{3+} ions. Classical model calculations of these fragmentation processes have been reported recently [14], while quantum mechanical treatment is still a challenge. In parallel, Alexander *et al.* [15] reported photodissociation of D_3^+ that was allowed to vibrationally cool by storage in an electrostatic trap. They found that the dissociation rate decreased as D_3^+ cooled suggesting that, under the laser conditions used, dissociation is dominated by excited vibrational states.

In many ways the study of the dissociation of D_3^+ is more insightful than exploring the ionization channels. By avoiding ionization, only the nuclear dynamics of D_3^+ need to be treated by theory making it computationally more manageable although still very challenging. The D_3^+ ion also has a rather unusual geometry, forming an equilateral triangle in its unperturbed ground state. When dressed with an intense laser, the D_3^+ electronic ground state, $X\,^1A'$, is coupled with the first excited state, which in C_s symmetry (isosceles triangle) is $2\,^1A'$. These states lead to different two-body dissociation limits, $D^+ + D_2(X\,^1\Sigma_g^+)$ and $D(1s) + D_2^+(X\,^2\Sigma_g^+)$, respectively. Alternatively, in D_{3h} symmetry (equilateral triangle), the first excited state, $1\,^1E'$, and ground state lead to the degenerate three-body dissociation limit forming $D^+ + D(1s) + D(1s)$.

These properties of the D_3^+ molecule raise many questions. For example, which way does the molecule prefer to dissociate, i.e., to the two- or the three-body dissociation limit? Is the breakup energetic or not? What are the dissociation pathways involved?

In this paper we provide answers to some of these questions by exploring the dissociation of D_3^+ in intense ultrashort (10–40 fs), 790- and 395-nm laser pulses (atomic units are used throughout unless otherwise specified). Using the kinetic energy release (KER) distributions from dissociation we determine the most likely dissociation pathways. We also reassess the dissociation-path assignments suggested by Alexander *et al.* [15], whose measurements were limited to time of flight of the neutral fragments without being able to distinguish different dissociation channels (namely $D^+ + D_2$, $D_2^+ + D$, or $D^+ + D + D$). Finally, we assert a form of control over the D_3^+ dissociation through influencing the pathway by means of the pulse duration.

II. EXPERIMENTAL METHOD

Our experimental method is a modified version of the one used in our earlier studies of laser–molecular-ion interactions [16–18]. We have improved the method so that we can perform three-particle, as well as two-particle, coincidence measurements [13] and thereby image the fragmentation of D_3^+ into both two and three bodies. Recently the apparatus has also been upgraded specifically to measure very low-KER fragments (near 0 eV) in addition to the higher-KER fragments that could previously be measured [19,20].

We use a Ti:sapphire laser system with a fundamental wavelength of 790 nm providing linearly polarized 25-fs pulses [full width at half maximum (FWHM)] with 2-mJ energy at a repetition rate of 2 kHz. For ultrashort pulse generation these pulses are compressed using a neon-filled hollow-core fiber and chirped mirror arrangement that results in sub 10-fs (FWHM) pulses [21]. Second harmonic pulses at 395 nm can optionally be produced by passing the fundamental beam through a second harmonic generation crystal [beta-barium borate (BBO)]. In this case the output light from the BBO is separated using a dichromatic beam splitter that transmits the 395-nm light and reflects the 790-nm light. In the experiments the pulses are focused onto the ion beam target using an

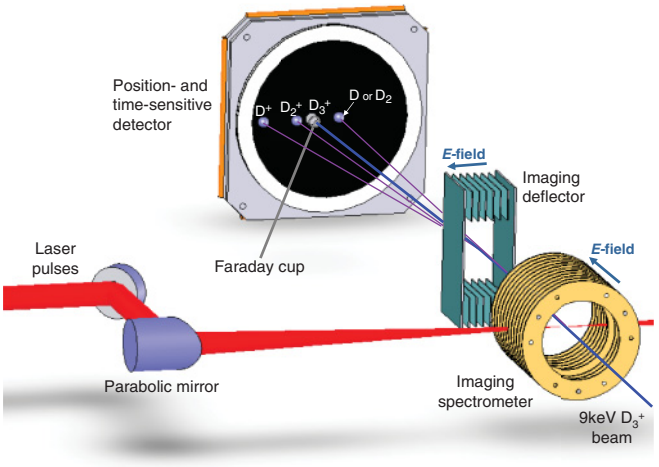

FIG. 1. (Color online) Schematic of the experimental setup.

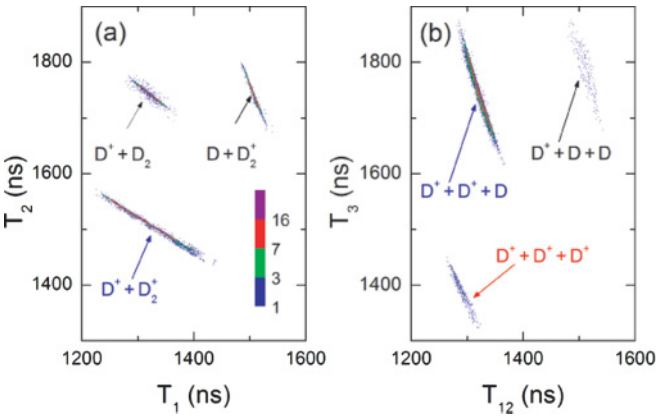

FIG. 2. (Color online) Coincidence time-of-flight (CTOF) map for the fragmentation channels of D_3^+ using 10-fs, 790-nm laser pulses with peak intensity of 10^{16} W/cm^2. (a) A density plot of two-body breakup as a function of the TOF of the first (T_1) and second (T_2) particles. (b) A density plot of three-body breakup as a function of the TOF of the center of mass of the first two particles (T_{12}) and of the third particle (T_3).

$f = 203$ mm off-axis parabolic mirror. The laser polarization is usually aligned along the ion beam direction in order to reduce the spot size of the molecular fragments hitting the detector, by taking advantage of the fact that most breakup processes favor alignment parallel to the laser field [11–13].

A collimated, mass-selected, 9-keV D_3^+ ion beam serves as the target in our present measurements (see additional experimental details in our previous publications, e.g., [13,16,17]). This D_3^+ beam is crossed with the focused laser beam at the interaction region, which is located inside a coaxial electrostatic spectrometer. The static electric field of the spectrometer is along the ion beam direction and acts to generate a time-of-flight (TOF) separation of the fragments according to their charge-to-energy ratio. This setup by itself (see [16]) has the drawback of losing very low kinetic energy fragments as they do not have enough transverse momentum to emerge out of the ion beam, which is captured in a small on-axis Faraday cup in front of the imaging detector. (This cup is needed to protect the detector and monitor the beam current during the experiment).

Therefore, to eliminate these losses of low-KER fragmentation we have recently added a parallel-plate deflector, which produces a static electric field perpendicular to the ion beam direction, between the interaction region and the detector [19,20]. This field separates the fragments spatially from the main beam and also from each other according to their charge-to-energy ratio, as shown in Fig. 1. Most importantly, it acts to pull the low-KER fragments out of the primary D_3^+ beam and the Faraday cup, without losing the imaging capabilities of the previous setup. Thus, with this improved setup [i.e., applying a field on both the spectrometer and the deflector (of about 285.7 and 26.6 V/cm, respectively)], we can extend our previous imaging measurements of molecular breakup down to zero KER, within the detector resolution.

The coincidence three-dimensional molecular dissociation imaging method used here is similar to the one used previously [13,16,17], and further details on the implementation of this improved method are given elsewhere [19,20]. Briefly, the TOF and position of all the fragments (including neutral fragments, but excluding free electrons) are measured in coincidence using a microchannel plate detector with delay line anode readout operated in an event-by-event mode. From this information we reconstruct the full three-dimensional momenta of all the molecular fragments, thus retrieving the angular and KER distributions of dissociation and ionization—for the complete KER range.

Example coincidence TOF spectra for laser-induced fragmentation of D_3^+ are displayed in Fig. 2 for 9-keV beam energy with the spectrometer voltage set to 1000 V (285.7 V/cm). One can see that each fragmentation channel is nicely separated from the others. In addition, the plot indicates the relative yield of the corresponding channel (e.g., three-body dissociation to $D^+ + D + D$ is the weakest channel in Fig. 2).

It is important to note that the D_3^+ beam is produced in an electron cyclotron resonance (ECR) ion source by electron impact ionization of D_2 gas followed by the $D_2^+ + D_2 \rightarrow D_3^+ + D$ reaction (e.g., [22]). These D_3^+ ions, being the target in our experiment, are vibrationally excited (i.e., "hot"). The approximate vibrational population distribution evaluated by Anicich and Futrell [22] for this D_3^+ production reaction is peaked at an energy of about 2 eV above the minimum of the D_3^+ potential energy surface—a fact that plays a key role in the likely dissociation paths, as discussed below.

III. RESULTS AND DISCUSSION

Fragmentation of D_3^+ in a strong laser field leads to two- and three-body breakup, as shown in Fig. 2. The dissociative two-body breakup channels are

$$\begin{aligned} D_3^+ + n\omega &\rightarrow D^+ + D_2 \\ &\rightarrow D_2^+ + D, \end{aligned} \tag{1}$$

and the three-body breakup channel is

$$D_3^+ + n\omega \rightarrow D^+ + D + D, \tag{2}$$

where $n\omega$ denotes the multiphoton interaction with the strong laser field.

It is these dissociation channels that we concentrate on in this paper, where we measure the D_3^+ fragmentation using 10- and 25-fs, 790-nm laser pulses at intensities up to 10^{16} W/cm^2, and 40-fs, 395-nm laser pulses at intensities up to 5×10^{14} W/cm^2. For simplicity we only show the highest intensity results for each wavelength.

The first thing we note from our observations is that the yield of the three-body breakup into $D^+ + D + D$ is extremely low, as evident in Fig. 2 and from our earlier findings [13]. This is consistent with the deep D_3^+ potential well in D_{3h} symmetry, requiring absorption of at least five photons to initiate dissociation, by a $|X\,^1A'\rangle \rightarrow |1\,^1E'\rangle$ transition, from the $v = 15$ state. It has been shown that dissociation and ionization of D_3^+ by similar laser pulses is dominated by vibrational states around $v = 15$ (i.e., equilateral triangles with a deuteron-deuteron distance of about 3.2 a.u. [13]). Unfortunately, the low yield of this channel prevents its detailed study (e.g., the creation of a meaningful KER distribution). Therefore, from here on we focus only on the two-body dissociation channels.

Figure 3(a) shows the KER distributions for the two-body dissociation channels of D_3^+ for 10-fs, 790-nm laser pulses at 10^{16} W/cm^2. The figure shows that the $D^+ + D_2$ channel dominates over the $D_2^+ + D$ channel with a large peak around 0.1 eV. The KER distribution of this channel extends to above 1.5 eV, which is indicative of a second (or more) dissociation pathway contributing which involves the absorption of additional photons. In contrast, the $D_2^+ + D$ channel shows little-to-no events near 0 eV (inset). Instead it has a rather broad distribution peaked at ~0.8 eV that extends to above 1.5 eV, like the other channel.

A. Two-body dissociation pathways

To determine which dissociation pathways can lead to these KER distributions, we survey the light-dressed states (Floquet diagram) [23,24] of D_3^+ as plotted in Fig. 4. The potential curves have been calculated by Talbi and Saxon [25] for C_s symmetry (isosceles) where the internuclear separation of two of the nuclei is fixed (r) while the distance between their midpoint and the third nucleus (R) is stretched. For each value of R, Talbi and Saxon calculate the diatomic internuclear separation r that minimizes the potential energy (i.e., they evaluate the reaction path of the two-body breakup). The light-dressed state diagram, shown in Fig. 4, is simplified by considering only the lowest two states in the C_s symmetry (ground $X\,^1A'$ and first-excited $2\,^1A'$), because it takes at least eight photons to excite the next manifold of states while the $2\,^1A'$ can be excited by two photons—a similar argument is commonly used when treating H_2^+ dissociation in a strong field [11,12]. In the light-dressed states picture each of the potential curves is dressed (shifted) by the number of absorbed photons (n), denoted by $-n\omega$, where ω refers to the energy of a 790-nm photon. For example, the $2\,^1A'$ state dressed by two photons is labeled as $|2^1A' - 2\omega\rangle$. Where curves cross one another, transitions from one state to the other are most likely. The dissociation limit of the $X\,^1A'$ state is $D^+ + D_2$ while that of the $2\,^1A'$ state is $D_2^+ + D$, thus the final electronic state, $X\,^1A'$ or $2\,^1A'$, can be identified by the measured channel. An estimate of the KER can easily be found by evaluating the difference in energy between the initial energy and the final

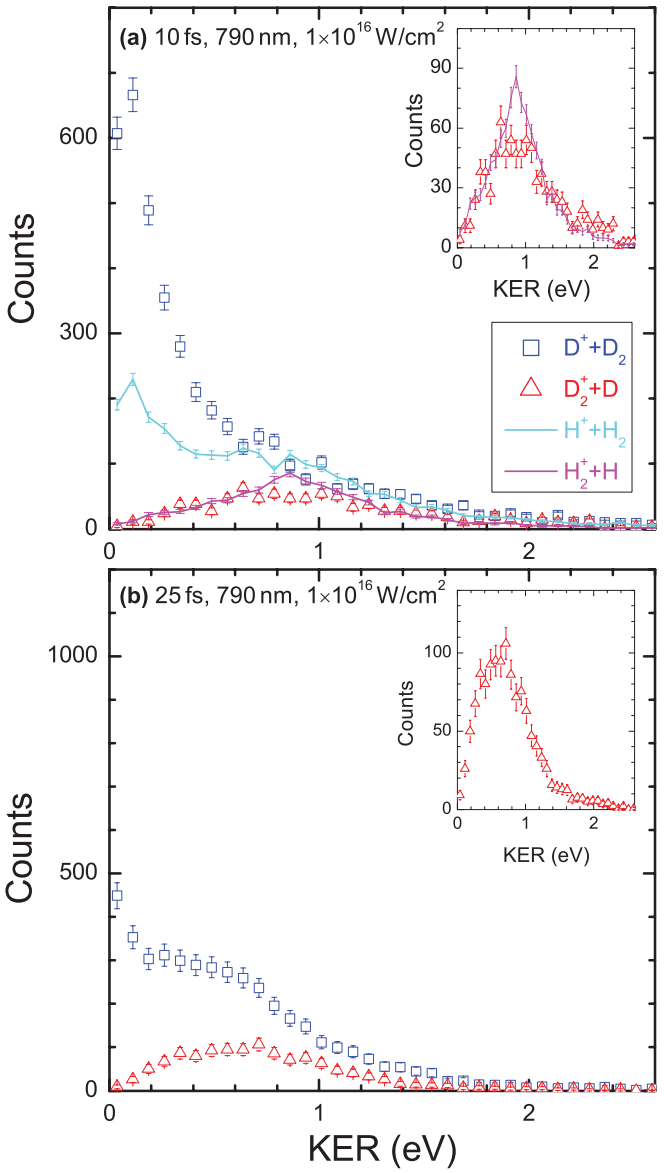

FIG. 3. (Color online) KER distributions for the two-body dissociation of D_3^+ using (a) 10- and (b) 25-fs, 790-nm laser pulses at an intensity of 10^{16} W/cm^2. Open blue squares are for the $D^+ + D_2$ channel and open red triangles are for the $D_2^+ + D$ channel. The lines in (a) are the equivalent for H_3^+. The error bars indicate the statistical uncertainty in the experimental data. The counts in (a) and (b) are normalized to the same number of target molecules per laser pulse and (b) is then scaled to visually match the peaks of the $D_2^+ + D$ channel in both panels to aid comparison. The insets of (a) and (b) show an expanded view of the $D_2^+ + D$ channel.

dissociation limit. For example, a few energies (i.e., KER) relevant to the current work are marked by the vertical arrows in Fig. 4. However, we do emphasize that these energies will only be approximate as bond softening [26] can lead to dissociation of vibrational (v) states above and below the initial crossings which in turn leads to higher and lower KER values observed. Additionally, the diatomic fragment (D_2 or D_2^+) may end up vibrationally excited thereby lowering the KER measured.

The large peak at 0.1 eV in the $D^+ + D_2$ KER distribution is most likely due to the dissociation pathway yielding

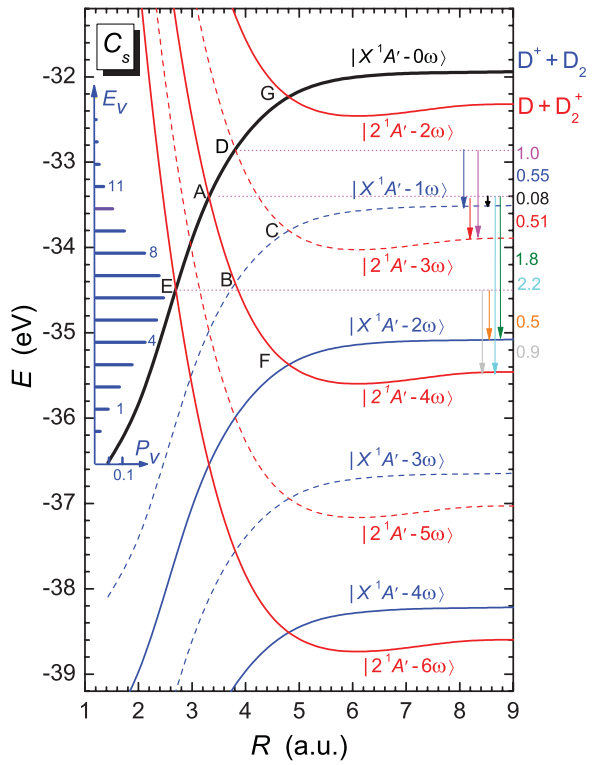

FIG. 4. (Color online) Light-dressed potential energy curves of D_3^+ where the potentials have been calculated in [25] for the C_s symmetry (isosceles triangle configuration). For this isosceles geometry, R is the distance between the midpoint of two of the nuclei and that of the third nucleus (see text). The ground $X\,^1A'$ electronic state leads to the $D^+ + D_2$ dissociation limit ($R \to \infty$) and the $2\,^1A'$ first excited electronic state leads to the $D_2^+ + D$ limit. The plot shows the dressed states for 790 nm, where ω refers to the energy of a 790-nm photon. To interpret the 395-nm (2ω) data only the solid-line curves should be considered. The vertical arrows indicate the KER (in eV) for a selection of dissociation pathways (see text). Inset (within the potential well) shows the energies and approximate population of the D_3^+ vibrational states evaluated by Anicich and Futrell [22] for the $D_2^+ + D_2 \rightarrow D_3^+ + D$ reaction creating D_3^+ in the ion source.

the lowest KER value, specifically $|X\,^1A'-0\omega\rangle \to |2\,^1A'-4\omega\rangle \to |X\,^1A'-1\omega\rangle$—yielding about 0.08 eV (see the A to B through C path in Fig. 4). The $D^+ + D_2$ channel can also be populated by a few other pathways yielding different KER values. For example, $|X\,^1A'-0\omega\rangle \to |2\,^1A'-3\omega\rangle \to |X\,^1A'-1\omega\rangle$ gives a KER of about 0.55 eV (D to C path), or $|X\,^1A'-0\omega\rangle \to |2\,^1A'-4\omega\rangle \to |X\,^1A'-2\omega\rangle$ which gives a KER of about 1.8 eV (A through B to F path), as well as others (see Fig. 4). This multitude of pathways is responsible for the KER tail extending to higher values in Fig. 3(a). The relative importance of the competing dissociation pathways depends on the number of photons involved, the coupling between the states, and the initial vibrational population of the D_3^+ near the curve crossing where each dissociation path begins. Indeed, the likely reason that the pathway yielding about 0.08 eV (initiated at A in Fig. 4) dominates over the pathway yielding 0.55 eV (starting at D in Fig. 4), discussed above, is because its crossing is accessing lower v states (v∼10–11 rather than v∼12–13) that have higher populations (see Fig. 4 and Ref. [22] for the population and energy of the D_3^+ vibrational states).

It is also important to note that vibrational excitation of the D_2 final product is not included in the potential energy curves shown in Fig. 4. This energy can be significant given that the initial D-D separation in the D_3^+ is much larger than the D_2 bond length, therefore the KER is expected to be lower than the values evaluated from Fig. 4 above. Moreover, this will cause an additional spread of the KER distribution.

By similar deduction, the pathways that can account for the $D_2^+ + D$ KER distribution are the $|X\,^1A'-0\omega\rangle \to |2\,^1A'-4\omega\rangle \to |X\,^1A'-1\omega\rangle \to |2\,^1A'-3\omega\rangle$ (i.e., the A to B to C path in Fig. 4) and the $|X\,^1A'-0\omega\rangle \to |2\,^1A'-3\omega\rangle$ (the D through C path in Fig. 4), roughly giving KER values of 0.51 eV and 1.0 eV, respectively. At first sight it may seem strange that the $D_2^+ + D$ channel does not have a sizable feature near 0.1 eV arising from the two-photon pathway $|X\,^1A'-0\omega\rangle \to |2\,^1A'-2\omega\rangle$ (i.e., the lowest possible photon-order process in D_3^+ dissociation). However, considering the negligible vibrational population near the $|X\,^1A'-0\omega\rangle$—$|2\,^1A'-2\omega\rangle$ crossing (see G in Fig. 4), it becomes apparent why this dissociation path barely contributes to the $D_2^+ + D$ KER spectrum shown in Fig. 3(a).

B. Control and confirmation of dissociation paths

We have further tested the assignment of pathways described above and, more importantly, demonstrated control over the low-KER dissociation path of D_3^+ by adjusting the pulse duration as described below and demonstrated previously by our group for H_2^+ [27].

First, the dissociation pathway yielding low KER $D^+ + D_2$ fragmentation proceeds from the curve crossing marked A in Fig. 4 to the one marked C (via B) eventually ending on the $|X\,^1A'-1\omega\rangle$ state. A classical estimate indicates that it takes a nuclear wave packet about 11 fs to travel between these A and C crossings. If the laser pulse is shorter than the travel time along this path, one would expect the dissociating wave packet to remain on the $|X\,^1A'-1\omega\rangle$ state rather than transit to the $|2\,^1A'-3\omega\rangle$ curve, because the crossing at C is likely to be closed when it reaches it (note that the curve crossings are laser induced and are only open in the presence of a strong laser field). This dissociation path involving transitions at the crossings marked A and B in Fig. 4, while remaining on the same curve while passing the crossing C, is in accord with our findings of an enhanced low-KER dissociation into $D^+ + D_2$ for a 10-fs laser pulse shown in Fig. 3(a). Moreover, this suggests that this low-KER dissociation process should be reduced, for example, by conducting similar measurements but with a 25-fs pulse. The low KER in the $D^+ + D_2$ channel is clearly reduced in comparison with the rest of the distribution, shown in Fig. 3(b), supporting the above argument. Naturally one would expect a corresponding signal increase in the $D_2^+ + D$ channel around 0.51 eV, as the wave packet made a transition at C to the $|2\,^1A'-3\omega\rangle$ state. The inset in Fig. 3 suggests an increase by about a factor of 2, however, caution is advised when comparing these insets due to the difficulty in normalizing the two measurements exactly to each other.

Second, the dependence on the travel time between the curve crossings along the dissociation pathway can also be

probed by changing the speed of the nuclear wave packet while keeping the pulse duration fixed (at 10 fs here). This can be accomplished by comparing the dissociation dynamics of different isotopes [27], in this case H_3^+ [lines in Fig. 3(a)] to D_3^+ (symbols in the same figure). In this scenario the nuclear wave packet travels $\sqrt{2}$ times faster for the lighter H_3^+ than the D_3^+, thus reducing the travel time between crossings. As a result, for 10-fs laser pulses, more of the wave packet traveling from A to C is transferred to the $|2\,^1A' - 3\omega\rangle$ state via crossing C for H_3^+ than for D_3^+ resulting in the observed (see Fig. 3) drop in the low-KER yield for the $H^+ + H_2$ channel and corresponding increase in yield in the $H_2^+ + H$ channel (albeit at slightly higher KER than the estimated 0.51 eV).

Third, another convenient way to verify the dissociation pathways assigned in our discussion above is to use 395-nm light, the results of which are shown in Fig. 5. Since the photon energy is doubled at this wavelength (i.e., one 395-nm photon is equivalent to 2ω), one effectively eliminates the states involving an odd number of (790-nm) photons—the remaining curves, relevant in this case, are shown as solid lines in the light-dressed states pictured in Fig. 4. It is clear that the pathways discussed for 790 nm are now absent altogether, which results in the distinct reduction in the low-KER feature in the $D^+ + D_2$ channel at 395 nm. The most likely pathways in this case are $|X\,^1A' - 0\omega\rangle \rightarrow |2\,^1A' - 6\omega\rangle \rightarrow |X\,^1A' - 2\omega\rangle$ and $|X\,^1A' - 0\omega\rangle \rightarrow |2\,^1A' - 6\omega\rangle \rightarrow |X\,^1A' - 2\omega\rangle \rightarrow |2\,^1A' - 4\omega\rangle$—giving estimated KER values of about 0.5 eV and 0.9 eV, respectively. The actual distributions for the $D^+ + D_2$ and $D_2^+ + D$ channels (Fig. 5) consistently peak slightly higher which, as before, can arise from dissociation of v states above the initial $|X\,^1A' - 0\omega\rangle$—$|2\,^1A' - 6\omega\rangle$ crossing, labeled E in Fig. 4. In fact, our measurement of the relative dissociation rate at 395 nm is substantially higher than at 790 nm (about a factor of 50) in spite of the much lower peak intensity. This is most likely due to the lower number of photons needed to initiate dissociation, and the higher vibrational population near the E crossing (see Fig. 4).

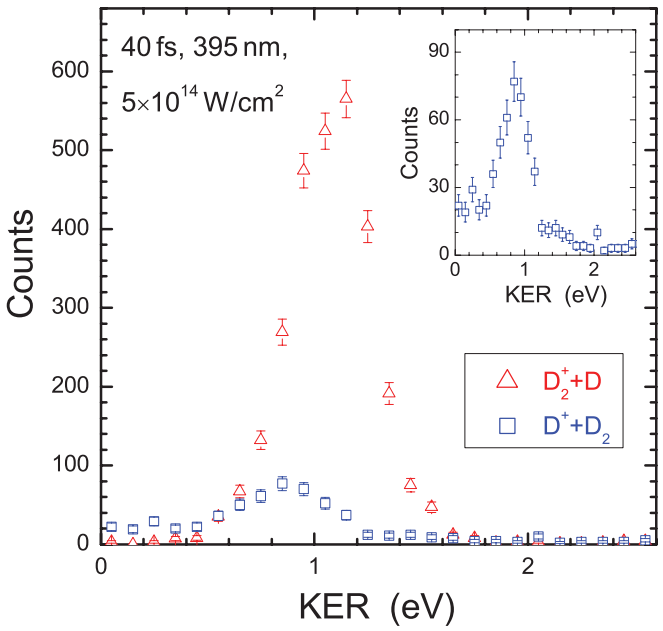

FIG. 5. (Color online) KER distributions for the two-body dissociation of D_3^+ using 40-fs, 395-nm laser pulses at an intensity of 5×10^{14} W/cm^2. The inset shows an expanded view of the $D^+ + D_2$ channel. The error bars indicate the statistical uncertainty in the experimental data.

C. Comparison to previous work

It is worth commenting on the recent findings of Alexander *et al.* [15], who also measured the strong-field (30 fs, 800 nm at 10^{14}–10^{16} W/cm^2) dissociation of D_3^+, allowing the molecules to vibrationally cool over tens of milliseconds in an ion trap. Unfortunately, this scheme only allowed measurement of the time of flight of neutral fragments without determining their identity (i.e., D or D_2). Alexander *et al.* found that their TOF spectra were dominated by a very low-energy peak (near 0 eV), as in our measurements, that diminished as the molecules cooled. From the information available at the time, the authors postulated that dissociation most likely arose from a two-photon transition from the ground $X\,^1A'$ to the excited $2\,^1A'$ state (in C_s symmetry) leading to the $D_2^+ + D$ channel. In arriving at this conclusion, they did consider an alternative dissociation path leading to the $D^+ + D_2$ channel which involves a three-photon absorption followed by two-photon emission when R approaches 4.8 a.u. (i.e., the $|X\,^1A' - 0\omega\rangle \rightarrow |2\,^1A' - 3\omega\rangle \rightarrow |X\,^1A' - 1\omega\rangle$ dissociation path). They also speculated that at higher intensities the ionization channel $D^+ + D^+ + D$ may contribute to the formation of low-energy D fragments.

From what we have now learned from our own measurements, we can shed new light on the experiments of Alexander *et al.* [15]. The very low-KER dissociation ($\lesssim$0.1 eV) comes instead from four-photon excitation (from $X\,^1A'$ to $2\,^1A'$) followed by three-photon emission (from $2\,^1A'$ back to $X\,^1A'$)—a net one-photon process, with the final products being $D^+ + D_2$. This is in contrast to two-photon excitation from $X\,^1A'$ to $2\,^1A'$ leading to $D_2^+ + D$ that was suggested in [15]. In our view this two-photon pathway is unlikely as the crossing between the $X\,^1A'$ and $2\,^1A'$ states is about 4.3 eV above the D_3^+ potential minimum with the population in these high vibrational states likely to be extremely low (see Fig. 4).

The other dissociation path discussed by Alexander *et al.* [15], namely $|X\,^1A' - 0\omega\rangle \rightarrow |2\,^1A' - 3\omega\rangle \rightarrow |X\,^1A' - 1\omega\rangle$ that leads to $D^+ + D_2$, does appear in our measured KER spectrum shown in Fig. 3. It appears as a broad distribution centered at about 0.55 eV in accordance with the expected value from Fig. 4, and close to 0.4 eV (0.31 eV) as evaluated (measured) in Ref. [15] under the assumption that the detected neutral is a D_2. We further note that Fig. 3 shows that the relative contribution from this pathway increases with increasing pulse duration as the low-KER feature below 0.1 eV becomes less pronounced. Thus, for the conditions used in Ref. [15] (i.e., 30-fs pulses), this 0.55-eV pathway may well dominate.

We can also make a statement on the likelihood of the $D^+ + D^+ + D$ ionization channel contributing in the experiment in Ref. [15]. We find in our measurements that the D fragment from this channel typically has substantial nonzero energy, distributed around 2 eV, with overall channel KER of about 10 eV [13]. Hence, we do not expect it to make any contribution in the low-energy range where the peak for a neutral fragment was observed.

The insight we provide is founded on our ability to clearly distinguish the $D_2^+ + D$ and $D^+ + D_2$ channels, as well as all others (see Fig. 2). This allows us to determine that the peak near 0 eV is associated with the $D^+ + D_2$ channel rather than the $D_2^+ + D$ channel (see Fig. 3), or any other. This is a nice demonstration of the benefits of coincidence measurements. While one cannot rule out that different ion source or experimental conditions may lead to different behavior of D_3^+ in the two experiments, we would expect any differences to be more subtle.

IV. SUMMARY

In summary, following the recent development of our experimental method to be able to measure low (and high) KER fragments in coincidence, we have conducted a study of the dissociation dynamics of a D_3^+ molecular-ion beam in an intense ultrashort laser field. From the measured KER distributions and a light-dressed states picture of the D_3^+ potentials, the relevant dissociation pathways at 790 and 395 nm have been deduced. Indeed, we have shown that there are important time-dependent dynamics involved in the strong-field dissociation of this molecule, which we use to control the relative importance of the low-KER dissociation process by manipulating the pulse duration. Finally, with the benefit of coincidence measurements, we propose an amended interpretation of earlier D_3^+ dissociation data.

ACKNOWLEDGMENTS

We thank Z. Chang and his group members and C. W. Fehrenbach for assistance with the laser and ion beams, respectively. We also recognize useful discussion with J. B. Greenwood and co-workers on comparison of our experiment with that of Alexander *et al*. This work was supported by the Chemical Sciences, Geosciences, and Biosciences Division, Office of Basic Energy Sciences, Office of Science, US Department of Energy.

[1] M. Larsson *et al*., Phys. Rev. Lett. **70**, 430 (1993).
[2] G. Sundström *et al*., Science **263**, 785 (1994).
[3] S. Datz, G. Sundstrom, Ch. Biedermann, L. Broström, H. Danared, S. Mannervik, J. R. Mowat, and M. Larsson, Phys. Rev. Lett. **74**, 896 (1995).
[4] D. Strasser *et al*., Phys. Rev. Lett. **86**, 779 (2001).
[5] H. Kreckel *et al*., Phys. Rev. Lett. **95**, 263201 (2005).
[6] D. L. Montgomery and D. H. Jaecks, Phys. Rev. Lett. **51**, 1862 (1983).
[7] L. M. Wiese, O. Yenen, B. Thaden, and D. H. Jaecks, Phys. Rev. Lett. **79**, 4982 (1997).
[8] J. E. Mann, C. M. Laperle, J. D. Savee, and R. E. Continetti, Chem. Phys. Lett. **473**, 34 (2009).
[9] U. Galster, P. Kaminski, M. Beckert, H. Helm, and U. Muller, Eur. Phys. J. D **17**, 307 (2001).
[10] A. Carrington and R. A. Kennedy, J. Chem. Phys. **81**, 91 (1984).
[11] A. Giusti-Suzor *et al*., J. Phys. B **28**, 309 (1995).
[12] J. H. Posthumus, Rep. Prog. Phys. **67**, 623 (2004).
[13] J. McKenna, A. M. Sayler, B. Gaire, N. G. Johnson, K. D. Carnes, B. D. Esry, and I. Ben-Itzhak, Phys. Rev. Lett. **103**, 103004 (2009).
[14] E. Lötstedt,T. Kato, and K. Yamanouchi, Phys. Rev. Lett. **106**, 203001 (2011).
[15] J. D. Alexander *et al*., J. Phys. B **42**, 141004 (2009).
[16] I. Ben-Itzhak, P. Q. Wang, J. F. Xia, A. M. Sayler, M. A. Smith, K. D. Carnes, and B. D. Esry, Phys. Rev. Lett. **95**, 073002 (2005).
[17] P. Q. Wang, A. M. Sayler, K. D. Carnes, J. F. Xia, M. A. Smith, B. D. Esry, and I. Ben-Itzhak, Phys. Rev. A **74**, 043411 (2006).
[18] B. Gaire, J. McKenna, N. G. Johnson, A. M. Sayler, E. Parke, K. D. Carnes, and I. Ben-Itzhak, Phys. Rev. A **79**, 063414 (2009).
[19] B. Gaire, J. McKenna, F. Anis, A. M. Sayler, M. Zohrabi, J. J. Hua, N. G. Johnson, K. D. Carnes, B. D. Esry, and I. Ben-Itzhak (in preparation).
[20] B. Gaire, Ph.D. thesis, Kansas State University, 2011.
[21] H. Mashiko *et al*., Appl. Phys. Lett. **90**, 161114 (2007).
[22] V. G. Anicich and J. H. Futrell, Int. J. Mass Spectrom. Ion Phys. **55**, 189 (1983).
[23] X. He, O. Atabek, and A. Giusti-Suzor, Phys. Rev. A **38**, 5586 (1988).
[24] S.-I. Chu, J. Chem. Phys. **75**, 2215 (1981).
[25] D. Talbi and R. P. Saxon, J. Chem. Phys. **89**, 2235 (1988).
[26] P. H. Bucksbaum, A. Zavriyev, H. G. Muller, and D. W. Schumacher, Phys. Rev. Lett. **64**, 1883 (1990).
[27] J. McKenna *et al*., Phys. Rev. Lett. **100**, 133001 (2008); J. McKenna, F. Anis, A. M. Sayler, B. Gaire, N. G. Johnson, E. Parke, K. D. Carnes, B. D. Esry, and I. Ben-Itzhak, Phys. Rev. A **85**, 023405 (2012).